



HAL
open science

Optimal lifetime management strategy for Self-Reconfigurable Batteries

Jérôme Blatter, Vincent Heiries, Remy Thomas, Ghislain Despesse

► **To cite this version:**

Jérôme Blatter, Vincent Heiries, Remy Thomas, Ghislain Despesse. Optimal lifetime management strategy for Self-Reconfigurable Batteries. VTC2022-Spring - IEEE 95th Vehicular Technology Conference, IEEE, Jun 2022, Helsinki, France. DOI: 10.1109/VTC2022-Spring54318.2022.9860429, 10.1109/VTC2022-Spring54318.2022.9860429 . cea-03907562

HAL Id: cea-03907562

<https://cea.hal.science/cea-03907562>

Submitted on 20 Dec 2022

HAL is a multi-disciplinary open access archive for the deposit and dissemination of scientific research documents, whether they are published or not. The documents may come from teaching and research institutions in France or abroad, or from public or private research centers.

L'archive ouverte pluridisciplinaire **HAL**, est destinée au dépôt et à la diffusion de documents scientifiques de niveau recherche, publiés ou non, émanant des établissements d'enseignement et de recherche français ou étrangers, des laboratoires publics ou privés.

Optimal lifetime management strategy for Self-Reconfigurable Batteries

Jérôme Blatter
CEA-LITEN

Univ. Grenoble Alpes
F-38000 Grenoble, France
jerome.blatter@cea.fr

Vincent Heiries
CEA-LETI

Univ. Grenoble Alpes
F-38000 Grenoble, France
vincent.heiries@cea.fr

Rémy Thomas
CEA-LITEN

Univ. Grenoble Alpes
F-38000 Grenoble, France
remy.thomas@cea.fr

Ghislain Despesse
CEA-LETI

Univ. Grenoble Alpes
F-38000 Grenoble, France
ghislain.despesse@cea.fr

Abstract—Due to factory production discrepancies and different operation conditions, cells integrated in conventional battery systems are not similar. In a static series connection, the weakest cell limits the battery pack capacity. Self-reconfigurable batteries (SRB), where semiconductor switches allow cells to be connected or bypassed dynamically, are used to by-pass the weakest cell and so use the full battery capacity at any time. The in-line configuration even allows the direct generation of AC current without any power converter. This paper proposes an optimal lifetime management strategy for SRB generating AC current. A full battery cell model including ageing mechanisms is used to perform the minimization of the SRB capacity losses with the aim of demonstrating the SRB capabilities in terms of lifetime extension. A direct multi-shooting numeric method is used to solve the minimization problem on battery partial discharge, which is often encountered, like in the electric vehicle usage. Simulation results validate the proposed method and a major lifetime extension of 54% compared to conventional battery pack has been observed.

Index Terms—batteries, self-reconfigurable, optimal control, battery lifetime extension, modelling

I. INTRODUCTION

Electrification in combination with green energy production seems to be the most promising solution to address the critical issue of climate change. However, mobility and intermittent renewable energy production require the use of storage systems. Lithium-ion battery represents a key technological solution due to its features: high energy and power density, wide temperature range of operation and low self-discharge. Unfortunately, the production process tolerance leads to a capacity and impedance discrepancies of the battery cells, even between identical, brand-new cells from the same batch

[1]. In a traditional battery pack, cells are statically connected in series and in parallel to comply with voltage and current requirements. As a consequence, the weakest cell limits the entire battery pack [2]. In addition, the dispersion between cells increases during battery aging due to individual operating conditions of cells in the same battery pack [3] limiting more and more the battery by the weakest cell. Battery Management Systems (BMS) are then used to supervise and compensate some of this dispersion. Frequently, a charge balancing mechanism compensating coulometric efficiency dispersion is used, although the weakest cell remains a limitation for the battery autonomy during the discharge phase. In this context, self-reconfigurable (SRB) batteries include switches, allowing to bypass the weakest cell or even to adjust the overall cell layout based on cell's individual state [4]. Therefore, balancing can be done during the whole operating cycle of the battery. Optimal control is often introduced in order to reach the best performance regarding battery efficiency, autonomy and lifespan.

Different optimization approaches are proposed depending on two common types of SRB well defined in [4]. In the first type, the SRB aims to perform a continuous voltage source like conventional battery pack. This can be done by dynamically connecting submodules (SM), which is a single cell or multiple ones in a static combination. The SRB control is done by using more or less power from this SM. However, a compromise must be found between balancing and minimizing battery losses while respecting the voltage requirements [4]. This is performed in [5]–[8], where an optimal strategy between balancing and battery efficiency is found. Moreover, [9] shows that using SRB with balancing allows a lifetime extension of 16%. In the second type, SRB are continuously reconfigured to perform an AC output waveform. Generally, a Multilevel inverter (MLI) architecture is selected [4] and the SRB can be directly used to power an electric motor or to be connected to the power grid without needing an additional power inverter.

In most publication on the topic, control strategies are performed regarding the correction of capacity and temperature dispersions [5]–[8], [10]. Lifespan increase is then an indirect consequence of these controls. Therefore, this paper proposes to develop a control strategy which directly optimize the SRB lifetime. This study is based on the SRB introduced by [11]

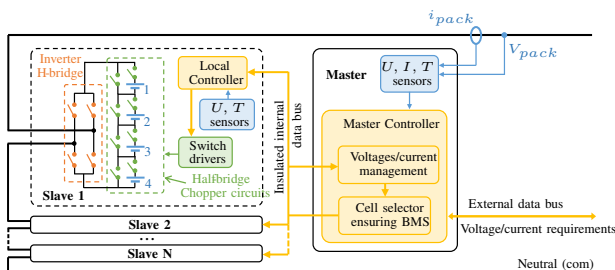


Fig. 1. SRB hardware architecture

and illustrated on Fig. 1, which corresponds to a topology of second type. In this SRB architecture, the SM is composed by a single cell that involves the use of many levels in the MLI architecture in order to respect the voltage requirement. Therefore, the Pulse Width Modulation becomes unnecessary to keep a low total harmonic distortion and the output voltage result in a staircase waveform. Then, the balancing can be performed with a sorting algorithm by assigning the strongest cell to the first voltage level corresponding to the highest average current, the second-strongest cell to the second voltage level and so on. It can be noted that, after several iterations, the strongest cells become among the weakest ones. Thus, a rotation of the cell level assignation is required to keep cells balanced.

Performing balancing for this type of SRB have the prospect to maximize the battery autonomy. However, in most cases, batteries are not fully discharged. In [12], the average travelling distance of private vehicles in some European cities are analysed. The mean covered distance of a single trip is between 7 and 20 km. The mean driven distance during one day is around 30 and 70 km. This is far from the presented autonomy of actual and future electric vehicles. The lifespan optimization could then be done on partial depth of discharge.

The aim of this paper is to present a methodology that use the full potential of SRB with the MLI architecture to extend the battery lifetime. Optimization is performed directly on the SRB's capacity loss so that the strategy reflects the best possible control concerning lifespan augmentation. Simulation of a SRB is used to validate the optimal control strategy.

This paper is organized as follows. In section II, the battery cell model used for this study is presented, including an electrical model, a thermal model and a Li-ion cell-ageing model. Section III formulates the optimization problem and tackles the issue of a great dimensionality. Then the problem is solved numerically with a direct multiple-shooting method. Section IV presents and analyses the simulation result of a SRB subjected to the optimal strategy. The same profile and strategy is then applied over the whole battery life allowing the evaluation of the lifetime extension. Finally, section V concludes the paper.

II. BATTERY CELL MODEL

The definition adopted for State of Charge (SoC), State of Health (SoH) and C_{rate} of a battery cell is given in Eq. (1) to (3).

$$SoC(t) = 100 - \frac{100}{3600(Q_{bol} - Q_{loss}(t))} \int_0^t i_{cell}(\tau) d\tau \quad (1)$$

$$SoH(t) = 100 \frac{Q_{bol} - Q_{loss}(t)}{Q_{bol}} \quad (2)$$

$$C_{rate}(t) = i_{cell}(t)/Q_{nom} \quad (3)$$

with Q_{loss} the cell capacity loss since the beginning of life, i_{cell} the current circulating through the cell, Q_{nom} the cell nominal capacity provided by the manufacturer and Q_{bol} the measured cell capacity at beginning of life. As mentioned

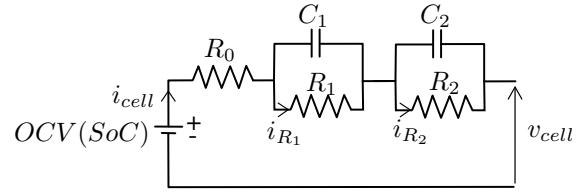


Fig. 2. 2-RC Thevenin Electrical Equivalent Circuit model

in the introduction, cells have capacity dispersion, even for brand-new cells. This is modelled by a normal distribution of cell's Q_{bol} in a battery pack around Q_{nom} .

A. Electrical model

Among the different battery models, Electrical Equivalent Circuit (EEC) bring a good compromise between model accuracy and computation complexity. A 2-RC Thevenin model (Fig. 2) has been chosen, with $R_1C_1 = 10s$ and $R_2C_2 = 100s$ [13]. The impedances R_j , $j \in \{0, 1, 2\}$ are not constant parameters regarding T , SoC , C_{rate} and SoH . So, multi-dimensional cartography obtained by hybrid pulse power characterization at different ageing progression is used to correct cell impedance according to this variable [4], [13].

B. Thermal model

The EEC model is used to calculate the generated heat [14]. Indeed, voltage drop reflect the cell losses and the thermal power is obtained with the joule effect of the impedances R_j (4). The cell thermal dynamic follows a simple heat diffusion model (5) with the assumption that cells are only cooled by air convection with the exterior at temperature T_{ext} and the convection coefficient h . C_p is the cell calorific capacity. Reversible heat generation is ignored [3].

$$P = R_0 i_{cell}^2 + R_1 i_1^2 + R_2 i_2^2 \quad (4)$$

$$C_p \dot{T} = P - h(T - T_{ext}) \quad (5)$$

C. Ageing model

In this paper, a semi-empirical capacity loss model developed during a previous project [13] is chosen. Equation (6) represents the degradation function law during cycling, mainly influenced by the Solid-Electrolyte Interphase growth that limit the ionic mobility of $Li+$. In addition, the ageing speed is adapted with the empirical function J dependent of the cell SoC , T and C_{rate} . α is an ageing accelerating factor when the cell reaches a certain point of capacity loss. A and m are experimental fitting coefficients. The empirical function, as well the parameters of the model, are identify by fitting the result of 6 cells continuously cycled at different T , SoC and C_{rate}

$$\dot{Q}_{loss} = \alpha \frac{J(C_{rate}, T, SoC)}{(1 + A Q_{loss})^m} |i_{cell}| \quad (6)$$

Calendar ageing is not taken into account because we suppose that during cycling, the capacity loss due to calendar

ageing is negligible compared to the capacity loss due to cycling ageing. And in this paper, only cycles are simulated.

III. OPTIMISATION PROBLEM

A. Statement of the problem

To fully show the potential of SRB concerning lifetime increase, global optimization over a well-known profile should be performed.

To address this issue, we used optimal control theory. An optimal control problem in the Bolza form is stated formally as follows:

$$\min_{u(t)} \mathbf{J} = \min_{u(t)} \int_{t_0}^{t_f} l(x(t), u(t), t) dt + \Phi(x(t_f)) \quad (7)$$

subject to the dynamic constraint

$$\dot{x}(t) = f(x(t), u(t), t) \quad (8)$$

and path constraint

$$g(x(t), u(t), t) = 0 \quad (9)$$

$$h(x(t), u(t), t) \leq 0 \quad (10)$$

with \mathbf{J} is the cost that must be minimized, t the time variable, l the running cost function, Φ the final cost function, f is the dynamic system differential function, g the equality constraint function and h the inequality constraint function. $x(t)$ and $u(t)$ are respectively the dynamic system's state vector and control vector.

Applied to the SRB, x is the combined state of every cell in the pack and it is defined as follows: $x = (\dots SoC_{cell} \dots i_{R1,cell} \dots i_{R2,cell} \dots Q_{loss,cell} \dots T_{cell} \dots)^T$ where $cell \in \{1, \dots, n\}$ and n the cell number in the battery pack. f is then defined by the combined dynamic of every cell model presented in section II : through the equations (1), (5), (6) and the model presented in Fig. 2.

The control vector $u = (\mu_1 \dots \mu_{cell} \dots \mu_n)^T$ represents the cell's connection state. If the cell is connected in series $\mu_{cell}(t) = 1$ or bypassed $\mu_{cell}(t) = 0$ in the SRB . So, the current circulating through the cell is defined by:

$$i_{cell}(t) = i_{pack}(t) \mu_{cell}(t) \quad (11)$$

$i_{pack}(t)$ is then the instantaneous current provided by the SRB and has for expression in our chosen application:

$$i_{pack}(t) = \sqrt{2} I_{rms}(t) \sin(\theta(t) + \phi(t)) \quad (12)$$

with $I_{rms}(t)$ the rms current, $\theta(t)$ the signal phase and ϕ the current phase-shift compared to the SRB output voltage.

After introducing the system state, dynamic and control, it is necessary to find the cost function that best meets the needs of the objective. Minimizing the battery pack capacity loss due to cycling ageing seems to be the simplest way to fulfil the system lifetime optimization. Only the capacity loss at the

end of the profile is considered. Capacity loss of the pack is estimated with the mean value of the cell capacity loss:

$$\mathbf{J} = \text{mean}_{cell}(Q_{loss}(t_f)) \quad (13)$$

We then chose to express $\Phi(x(t_f)) = \text{mean}_{cell}(Q_{loss}(t_f))^2$ and $l(x(t), u(t), t) = t^2 \text{mean}_{cell}(Q_{loss}(t))^2$ with a weighting that increase with time in order to return a more convex cost function and easier to solve problem.

Finally, for all battery pack using Li-ion cells, voltage limits of every cell must be respected. This can be included in the optimization problem with the inequality constraint function (10).

However, posing the problem in this way causes some issues. As mentioned in section I, SRB cell balancing is performed by a sorting algorithm that assigns the strongest cell to the first voltage level, the second-strongest cell to the second level, etc. This relatively simple algorithm can be iterated at a high rate, allowing to keep the SRB at a good balancing level. Performing optimization at the same time step leads to a problem with extremely high dimension.

B. Average current model

To decrease the dimension of the optimization problem, some assumption and simplification should be done.

The main hypothesis is that, optimization can be performed at a larger time step if a sorting algorithm is able to follow an average set point following the optimal strategy for each cell. This average control is then only limited by what the sorting algorithm is capable to perform. The sorting algorithm can be considered as a faster inner loop control.

The current circulating through the cell is now redefined by:

$$i_{cell}(t) = i_{av}(t) \mu_{cell}(t) \quad (14)$$

$$i_{av} = \frac{1}{\pi \cdot n} \sum_{cell} \int_0^\pi i_{cell}(\theta) d\theta \quad (15)$$

with i_{av} the average current in one period over all $cell$ and $\mu_{cell} \in \mathbb{R}$ now reflects the cell utilization rate.

An approximation of i_{av} can be done by considering the use of a FILO strategy (first-in last-out), where a cell is kept connected during the entire level utilisation in a half period of the AC signal. Other strategy can be use to perform the staircase waveform but the FILO strategy allows the greatest μ_{cell} dispersion if the reactive power is omitted. So, the maximal dispersion can be computed at the same time. In order to calculate i_{av} , the average current of one level must be first computed. Fig. 3 illustrates the staircase waveform of the SRB voltage output, which follows a reference sinusoidal signal expressed as:

$$V_{ref}(\theta) = \sqrt{2} U_{rms} \sin(\theta) \quad (16)$$

with U_{rms} the desired output rms voltage.

Each voltage step represents a new cell being connected. This voltage step is called *level*. V_{pack} is the voltage sum

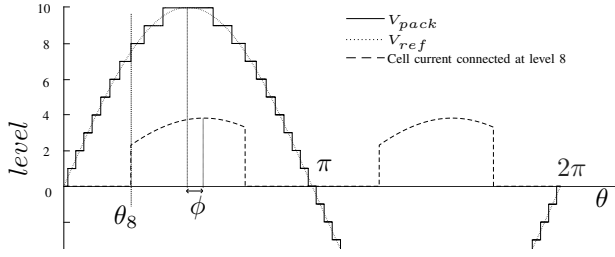


Fig. 3. Staircase waveform generated by SRB using a MLI architecture

of all connected cell. The voltage increase of a new level is approximated by the mean value of the cell voltage:

$$V_{pack} = level \underset{cell}{\text{mean}}(V_{cell}) \quad (17)$$

V_{pack} can also be calculated according to V_{ref} and θ_{level} , which is the angle at which the cell is connected to perform the staircase waveform (18). Using this equation, θ_{level} can be defined with (19). Eq. (20) gives the maximal value that $level$ can take.

$$V_{pack} = \sqrt{2} U_{rms} \sin(\theta_{level}) + 0.5 \underset{cell}{\text{mean}}(V_{cell}) \quad (18)$$

$$\theta_{level} = \arcsin((V_{pack} - 0.5 \underset{cell}{\text{mean}}(V_{cell})) / (\sqrt{2} U_{rms})) \quad (19)$$

$$level \in \mathbb{N} \mid 0 \leq (level - 0.5) \underset{cell}{\text{mean}}(V_{cell}) < \sqrt{2} U_{rms} \quad (20)$$

Then, the average current of a level i_{level} during one period is calculated according θ_{level} and the current flowing through the SRB at this moment (21). On Fig. 3 an example of the current flowing through the cell connected at the $level = 8$ is displayed. It is noticeable that the same cell is kept running during the entire level utilization. Equation (21) is the calculation of the average current according to the signal on a half-period with the FIFO strategy.

$$i_{level}(\theta_{level}) = \frac{2}{2\pi} \int_{\theta_{level}}^{\pi - \theta_{level}} \sqrt{2} I_{rms} \sin(\theta + \phi) d\theta \quad (21)$$

Finally, i_{av} is calculated with the mean value of i_{level} over each level (22).

$$i_{av} = \frac{1}{n} \sum_{level} i_{level} \quad (22)$$

With this definition of i_{av} , it is necessary to constrain the mean value of μ_{cell} to one in order to respect the amount of capacity consumed during utilization. Furthermore, μ_{cell} must be limited concerning the maximal dispersion that the SRB is capable to deal with. A useful dispersion indicator is the stochastic variance. So i_{cell} variance must be kept smaller than the variance of i_{level} and i_{cell} must be bounded with the maximal and minimal value of i_{level} . Eq. (23) summarizes all constraints on μ_{cell} .

$$\mathbf{C}(u) = \begin{cases} \underset{cell}{\text{mean}}(\mu_{cell}) = 1 \\ \mu_{cell} \geq \underset{level}{\min}(i_{level}/i_{av}) \\ \mu_{cell} \leq \underset{level}{\max}(i_{level}/i_{av}) \\ \underset{cell}{\text{var}}(\mu_{cell}) \leq \underset{level}{\text{var}}(i_{level}/i_{av}) \end{cases} \quad (23)$$

Unfortunately, using an average current for i_{cell} (14) invalidates the non-linear battery cell model. In particular, the heat generation in the thermal model (4), where i_{cell} is in square, has an important non-linear dynamic. Nevertheless, similarly to the calculation of i_{av} , an average power can be computed for joule effect associated with R_0 .

$$\begin{aligned} P_{R_0,level}(\theta_{level}) &= \frac{2 R_0}{2\pi} \int_{\theta_{level}}^{\pi - \theta_{level}} (\sqrt{2} I_{rms} \sin(\theta + \phi))^2 d\theta \\ P_{R_0,av} &= \underset{level}{\text{mean}}(P_{R_0,level}) \\ P_{R_0,cell} &= P_{R_0,av} \mu_{cell} \end{aligned} \quad (24)$$

The same remark applies for the ageing model (6). However, the empirical function J makes it difficult to evaluate the non-linearity. In addition, there are not enough publications showing that switching has an influence on cell lifetime [4], [15]. Therefore, the ageing model is unchanged concerning the average current model.

Finally, the optimization problem can be expressed here after :

$$\min_u \mathbf{J}(x(t_0)) = \min_u \int_{t_0}^{t_f} t^2 \underset{cell}{\text{mean}}(Q_{loss}(t))^2 dt + \underset{cell}{\text{mean}}(Q_{loss}(t_f))^2 \quad (25)$$

Subject to :

$$\dot{x}(t) = f(x(t), u(t), t) \quad (26)$$

$$2.5 \leq v_{cell}(x, t) \leq 4.2 \quad (27)$$

$$\mathbf{C}(u, t) \quad (28)$$

f also includes the average current model (14) and the average heat generation model of R_0 (24)

C. Resolution Algorithm

Regarding the cell model parameters cartography, the non-linear model and the number of constraints, a numeric resolution appears to be unavoidable. Direct multi-shooting method is used to convert the discrete dynamic optimal problem into a static optimization problem [16]. Then, common Non-linear programming (NLP) solver is efficient and represent an adapted choice. The simulation example in section IV are produced with solvers from the optimization toolbox of Matlab. Discretization is performed by solving linear time-variant system for the computation of SoC , i_{R_1} , i_{R_2} , and T . Q_{loss} is solved by performing the Euler method because the time step is chosen small in confrontation with the four other variables.

IV. SIMULATION RESULTS

As mentioned in section I, a lot of use cases only partially discharge batteries. Finally, a profile with a Depth of Discharge (DoD) of 25% is chosen. A battery pack of 25 cells is chosen for the simulation to illustrate the optimal strategy while keeping a visibility on every cell state and to have a decent computation time. The battery cell model comes from a $Q_{nom} = 2.9$ Ah Li-ions Nickel Manganese Cobalt (NMC) 18650 cell with graphite anode [13]. The corresponding ageing

speed function J , considered in this study, is represented in Fig. 4 where the dependence to SoC is shown for some representative value of C_{rate} and T . Additionally, the battery pack starts to be simulated with a normal distribution for cell's Q_{bol} and R_0 , with a standard deviation of respectively 1% and 6% [3]. Battery cell numeration is in the ascending order of the cell's Q_{bol} .

A. Test profile simulation

In this subsection, simulation is performed on a simple profile rule composed of the following three phases: constant power discharge, constant power charge and variable power charge. In the first phase, the SRB is discharged during 15 minutes with a constant rms current of $I_{rms}=6A$. In the second phase, the SRB is charged with a constant rms current of $I_{rms}=-2A$ until one cell voltage reaches the maximal allowed voltage: $\max(v_{cell}) = 4.2V$. In the last phase, rms current is calculated in such a way that the cell with the highest voltage is kept to 4.2V until the pack SoC reach 100%. During the whole profile, the SRB voltage signal is a sinus at rms voltage $U_{rms} = 44.2V$ and constant frequency. The current phase-shift stays at $\phi=0$.

Fig. 5 shows the simulated voltage, SoC , T and μ_{cell} of the SRB using the profile rule and no specific cell control. Each cell is used during the same amount of time. This means that the sorting algorithm performs a perfect rotation between cell. v_{cell} , SoC and T present some dispersions due to the initial dispersion of Q_{bol} and R_0 . The generated profile is called test profile.

Fig. 6 shows the simulation of the SRB using a control strategy obtained by solving the optimization problem stated in section III. The same test profile is used in both simulations to obtain exactly the same rms current profile. It can be observed through the behaviour of μ_{cell} that, the optimization is performed by using a limited number of the available SRB cells. In fact, the number of cells in the SRB is chosen to respect the output voltage when the cells are at minimum voltage : $\frac{2.5V \cdot 25}{\sqrt{2}} = 44.2V$. That means, the SRB only need

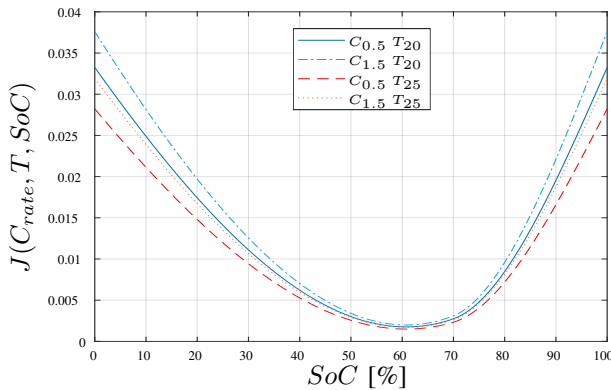


Fig. 4. Empirical ageing speed function of a 2.9A.h NMC Li-ions cell in relation to SoC at a combination of $T = 20^\circ C$, $T = 25^\circ C$, $C_{rate}=0.5$ and $C_{rate}=1.5$

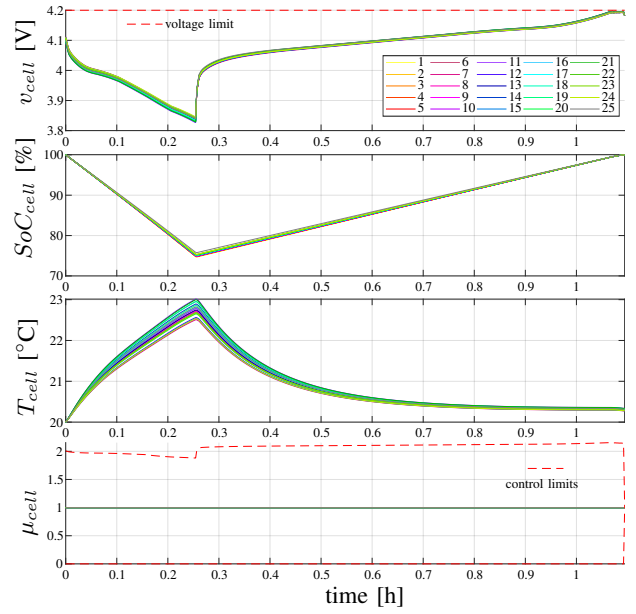


Fig. 5. Simulation of the test profile using no strategy

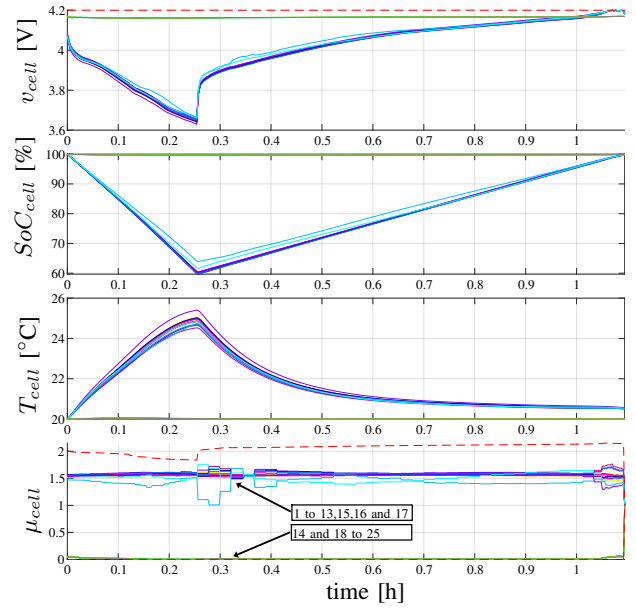


Fig. 6. Simulation of the test profile using optimal strategy

some cells when the SoC is high to provide the output voltage. At the end of the profile, it can be noted that the strategy is adapted to satisfy the voltage constraint reached at end of charge.

Fig. 7 exhibits a comparison of the battery capacity evolution along time between the two simulations. The optimization allows reducing by 29% the total capacity loss compared to the reference no strategy simulation. This benefit is explainable by the ageing speed function J illustrated in Fig. 4. The cycling ageing is mainly due to a high value of SoC , and so ageing gain is obtained by reaching as soon as possible an optimal SoC value, and then using some cells at lower SoC value as

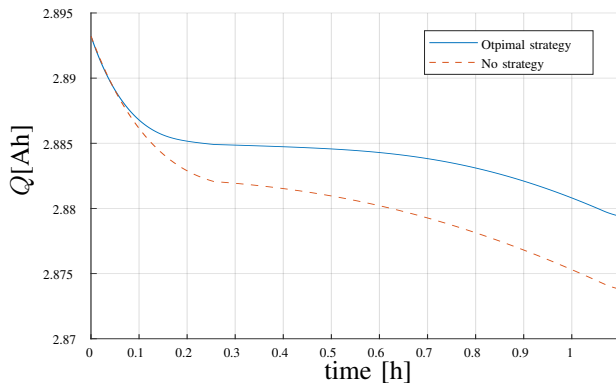


Fig. 7. Mean cell capacity comparison between the SRB using no strategy and optimal strategy during the simulation of the test profile

shown on Fig. 6 with the SoC_{cell} behaviour.

B. Whole lifespan simulation

By using a specific optimized control strategy on the test profile at the SRB begin of life, 29% capacity loss reduction are observed. One may ask if this benefit lasts over the whole SRB life. This is the subject of this subsection.

The whole SRB life can be simulated by cycling profiles like the one mentioned in the previous section and until a SoH threshold is reached. Between each cycle, the SRB SoC , i_{R1} , i_{R2} and T are reset to the initial condition. Only Q_{loss} are transferred from a cycle to the next one.

However, optimization over the whole lifetime is not possible due to the high dimension of the optimization problem. Suboptimal solution can be performed by optimizing each cycle separately. But, according to the equation (6), we see that ageing speed decreases with the increase of Q_{loss} . So, the optimal control strategy gives priority to the use of the cell with a more advanced ageing at a specific cycle. Consequently, during the cycling, the same group of cells are used and then these cells reaches the end of life before the others. A solution must be found so that every cell reach its end of life at the same time.

As explained above, the optimal solution showed in Fig. 6 is mainly impacted by the form of the empirical function J , which is the dependence of the ageing relatively to the SoC (Fig. 4). In return, the initial dispersion of cell parameters has low influence on the optimal control strategy. So, permuting the optimal control μ_{cell} between the cells have little effect on the capacity gain. Then, the assumption is done that the optimal solution between some consecutive cycles change little if the SoH is balanced. So, maintaining the same optimal control over some consecutive cycle leads to a near suboptimal solution. SoH balancing is obtained by permuting the control between cells at the beginning of each cycle. Optimization is then performed over one cycle at different SoH value to correct the optimal control. Q_{loss} at the beginning of a cycle can be calculated with equation (2).

In brief, optimal solutions are calculated on profiles dispatched every 2% of SoH. Then, the optimal control obtained at 100% of SoH is maintained over several cycles to reach 98% SoH. There, the control is replaced by the optimal solution obtained at 98% of SoH. Then, the control is maintained again over several cycles to reach 96% of SoH and so on. At each cycle beginning, the optimal control between cells is permuted in such a way that the cell SoH is kept balanced.

Fig. 8 shows the simulated v_{cell} , μ_{cell} and SoH_{cell} of the cycling using the optimal strategy from the SRB's beginning of life down to 97% of SoH . The SoH of the SRB using no strategy is also plotted. It can be seen that permuting the control μ_{cell} between cell keep the SoH balanced and that the constraints are almost respected. We can see that another control strategy is used when the SRB passes 98% of SoH according to the method mentioned above. The gap between optimal strategy simulation and no strategy simulation increase during ageing. So, it can be concluded that the method is a good approximation of the suboptimal strategy at every cycle.

In parallel, a reference simulation is produced by cycling the test profile using no strategy until it reaches SRB's end of life. For purpose of comparison, the optimal simulation also uses the test profile to compute rms current at the beginning of each cycle. So, both simulation have equivalent profile over the whole lifespan.

Fig. 9 displays SRB capacities of the no strategy simulation and the optimal strategy simulation during the whole lifetime. Taking the capacities at 5500 cycles, the capacity loss gain is now at 6.8%. We can conclude that capacity loss gain obtained by using the optimization framework previously described decreases during the SRB's life. If the SRB end of life is defined arbitrarily when the mean capacity value of the cells reach 2.1 Ah (72% SOH), it can then be seen that the no strategy simulation performs 5500 cycles and the optimal strategy 7100 cycles. This represents a lifetime extension of 29%.

Knowing the benefits of the optimal strategy compared to no strategy for SRB, it would be interesting to compare this result to conventional battery pack. The balancing capabilities of SRB experimented in [17] are so important that it can be assumed that a voltage balancing extracts most of the energy of the SRB. The mean value of the cell capacity is then a good image of the battery pack capacity. On the other side, the conventional battery is limited by the weakest cell. We assume that the conventional battery capacity with exactly the same Li-on cell connected in series and using a DC/AC converter to provide the AC output signal, is represented by the cell with the lowest capacity in the SRB with no strategy. We also assume that the SRB with no strategy and the conventional battery pack have the same ageing speed.

The conventional battery end of life is observed at 4600 cycles. Finally, the SRB using the optimal strategy enables lifetime extension of 54% compared to the conventional bat-

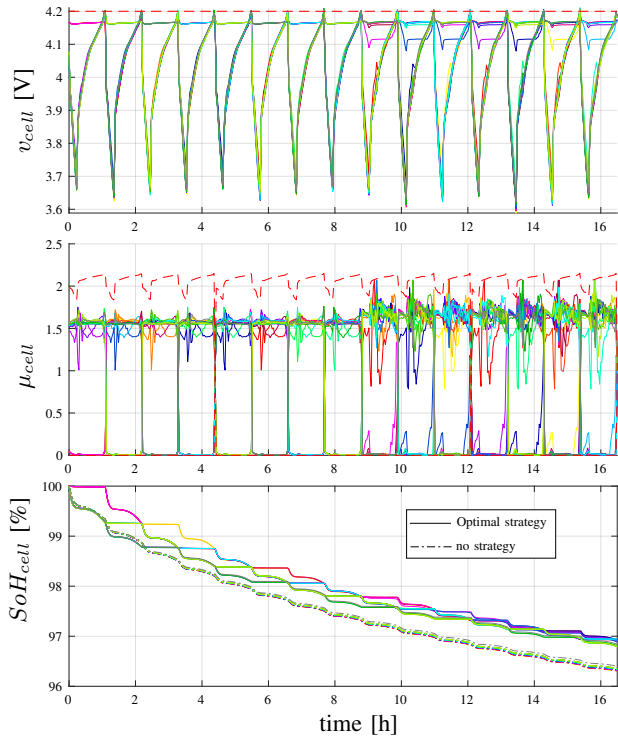


Fig. 8. Cycling simulation on the first 3% of SoH.

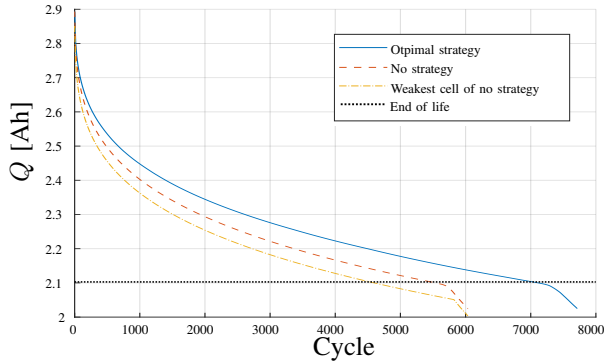


Fig. 9. Mean cell capacity comparison between the SRB using no strategy and optimal strategy during the whole lifetime. The weakest cell capacity of the SRB using no strategy is also plotted

tery.

V. CONCLUSION

This paper demonstrates the SRB capabilities to extend battery lifetime by using optimal control strategy. A complete battery cell model including cell ageing allows to perform the minimization on the battery capacity loss in a realistic framework. Solving the optimization problem on a simple partial discharge exhibits a major capacity loss reduction. Then, cycling this optimal control strategy over the battery life results in a significant lifespan augmentation compared to SRB using no specific control strategy and conventional battery pack.

Using the method described in this work on more realistic profiles, like the WLTP driving cycle or real world profile, will be the topic of future papers. Furthermore, this work can be used to evaluate the performance and give some clues for the development of real time control.

REFERENCES

- [1] K. Rumpf, A. Rheinfeld, M. Schindler, J. Keil, T. Schua, and A. Jossen, "Influence of Cell-to-Cell Variations on the Inhomogeneity of Lithium-Ion Battery Modules," *Journal of The Electrochemical Society*, vol. 165, no. 11, pp. A2587–A2607, 2018.
- [2] L. Lu, X. Han, J. Li, J. Hua, and M. Ouyang, "A review on the key issues for lithium-ion battery management in electric vehicles," *Journal of Power Sources*, vol. 226, pp. 272–288, 2013.
- [3] S. Paul, C. Diegelmann, H. Kabza, and W. Tillmetz, "Analysis of ageing inhomogeneities in lithium-ion battery systems," *Journal of Power Sources*, vol. 239, pp. 642–650, 2013.
- [4] L. Komsijska, T. Buchberger, S. Diehl, M. Ehrensberger, C. Hanzl, C. Hartmann, M. Hölzle, J. Kleiner, M. Lewerenz, B. Liebhart, M. Schmid, D. Schneider, S. Speer, J. Stöttner, C. Terbrack, M. Hinterberger, and C. Endisch, "Critical Review of Intelligent Battery Systems: Challenges, Implementation, and Potential for Electric Vehicles," *Energies*, vol. 14, no. 18, p. 5989, Sep. 2021.
- [5] N. Bouchhima, M. Schierle, S. Schulte, and K. P. Birke, "Active model-based balancing strategy for self-reconfigurable batteries," *Journal of Power Sources*, vol. 322, pp. 129–137, Aug. 2016.
- [6] A. Mondoha, J. Sabatier, P. Lanusse, S. Tippmann, and C. Farges, "Nonlinear Model Predictive Control for a Simulated Reconfigurable Battery Pack," *IFAC-PapersOnLine*, vol. 54, no. 6, pp. 353–358, 2021.
- [7] J. Kleiner, L. Lechermann, L. Komsijska, G. Elger, and C. Endisch, "Thermal behavior of intelligent automotive lithium-ion batteries: Operating strategies for adaptive thermal balancing by reconfiguration," *Journal of Energy Storage*, vol. 40, p. 102686, Aug. 2021.
- [8] F. Altai, B. Egardt, and L. Johannesson, "Electro-thermal Control of Modular Battery using Model Predictive Control with Control Projections," *IFAC-PapersOnLine*, vol. 48, no. 15, pp. 368–375, 2015.
- [9] N. Bouchhima, M. Gossen, S. Schulte, and K. P. Birke, "Lifetime of self-reconfigurable batteries compared with conventional batteries," *Journal of Energy Storage*, vol. 15, pp. 400–407, Feb. 2018.
- [10] M. Quraan, T. Yeo, and P. Tricoli, "Design and Control of Modular Multilevel Converters for Battery Electric Vehicles," *IEEE Transactions on Power Electronics*, vol. 31, no. 1, pp. 507–517, Jan. 2016.
- [11] R. Thomas, G. Despesse, S. Bacquet, E. Fernandez, Y. Lopez, P. Ramahefa-Andry, and L. Cassarino, "A high frequency self-reconfigurable battery for arbitrary waveform generation," *World Electric Vehicle Journal*, vol. 12, no. 1, pp. 1–12, 2021.
- [12] E. Paffumi and G. Martini, "Real-World Mobility and Environmental Data for the Assessment of In-Vehicle Battery Capacity Fade," *World Electric Vehicle Journal*, p. 17, 2021.
- [13] A. Laurin, V. Heiries, and M. Montaru, "State-of-Charge and State-of-Health online estimation of Li-ion battery for the More Electrical Aircraft based on semi-empirical ageing model and Sigma-Point Kalman Filtering," in *2021 Smart Systems Integration (SSI)*, Apr. 2021, pp. 1–4.
- [14] C. Forgez, D. Vinh Do, G. Friedrich, M. Morcrette, and C. Delacourt, "Thermal modeling of a cylindrical LiFePO₄/graphite lithium-ion battery," *Journal of Power Sources*, vol. 195, no. 9, pp. 2961–2968, May 2010.
- [15] K. Uddin, A. D. Moore, A. Barai, and J. Marco, "The effects of high frequency current ripple on electric vehicle battery performance," *Applied Energy*, vol. 178, pp. 142–154, Sep. 2016.
- [16] A. Rao, "A Survey of Numerical Methods for Optimal Control," *Advances in the Astronautical Sciences*, vol. 135, Jan. 2010.
- [17] R. Thomas, F. Lehmann, J. Blatter, G. Despesse, and V. Heiries, "Performance analysis of a novel high frequency self-reconfigurable battery," *World Electric Vehicle Journal*, vol. 12, no. 1, pp. 1–12, 2021.